




Cite this: *J. Mater. Chem. A*, 2022, 10, 19852

# A metal–organic framework-modified separator enables long cycling lithium-ion capacitors with asymmetric electrolyte design†

Yunlong Zhang, Yanan Li, Xiaoshan Wang, Xiaoling Teng, Lu Guan, Hao Yang, Zhengqiu He, Yi Wan,  Shiwei Guo, Han Hu \* and Mingbo Wu \*

The introduction of redox mediators, for example lithium iodide (LiI), into the catholyte of lithium-ion capacitors (LICs) could provide extra capacity through the iodide-involved redox reactions, allowing an alternative strategy to balance the huge capacity gap between the cathode and anode. Nevertheless, the formidable shuttle effect of the soluble mediators results in deteriorated cycling life. Herein, a metal–organic framework (MOF) interlayer is introduced to prohibit shuttling *via* physical obstruction and mild chemical attraction. After loading the MOF particles on the separator, the micropore of the MOFs could restrict the intragranular diffusion of the redox mediators while their intergranular migration could be prohibited by the mild chemical adsorption exerted by the MOF particles. The electrochemical evaluation reveals that the employment of the MOF-modified separator could boost the coulombic efficiency and cycling life of the activated carbon (AC) cathode with the LiI-included catholyte. Based on this discovery, a LIC was constructed by pairing the AC cathode with the LiI-involved catholyte and nanostructured  $\text{Li}_2\text{TiSiO}_5$  anode at the same mass loading where the MOF-modified separator is employed to prohibit the shuttle of iodine species. Because of the synergistic effects, such a LIC could offer a high energy, large power density, and long cycling life.

Received 21st March 2022  
Accepted 6th May 2022

DOI: 10.1039/d2ta02256g

[rsc.li/materials-a](https://rsc.li/materials-a)

## 1. Introduction

To counter severe anthropogenic global warming, clean and sustainable energy is actively pursued where energy storage systems (EESs) play an indispensable role.<sup>1–3</sup> Among all the available EESs, lithium-ion batteries (LIBs) and supercapacitors (SCs) are regarded as the most promising energy- and power-type devices, respectively. However, LIBs are limited in some practical applications due to their low power density ( $<1000 \text{ W kg}^{-1}$ ) and poor cycling performance (1000 cycles).<sup>4,5</sup> However on the other hand, SCs usually have excellent power density ( $>5000 \text{ W kg}^{-1}$ ) and long lifespan ( $>100\,000$  cycles) but are restricted by the low energy density ( $<10 \text{ W h kg}^{-1}$ ).<sup>6,7</sup> To explore a device that can simultaneously provide considerable energy density and power density, lithium-ion capacitors (LICs) have been extensively investigated.<sup>8</sup> A typical LIC comprises a capacitive cathode, for example activated carbon (AC), and a battery-type anode with a separator sandwiched between them. Unlike other types of devices, the two electrodes in LICs are operated using distinct mechanisms. As a result, the rational balance of

the gap between the two energy storage rules in the anode and cathode is of paramount importance.<sup>9–11</sup>

Generally, capacitive cathodes run with fast kinetics but a low capacity while battery-type anodes are just the opposite.<sup>12–14</sup> To reduce the kinetics imbalance, nanostructured materials with fast lithium-ion transfer capability, *e.g.* nanostructured  $\text{Li}_2\text{TiSiO}_5$  (LTSO), are needed to construct a battery-type anode.<sup>15–17</sup> To balance the capacity gap between the two electrodes, an overwhelming amount of cathode material is required. Based on the theoretical calculations, the loading mass of the cathode materials is 5 to 10 times higher than that of the anode materials. In this regard, the volume of the cathodes largely exceeds that of the anodes. Such a design will not only impose practical processing difficulty but also drastically decrease the performance of the LICs.<sup>18,19</sup> In addition to storing charges in electrode materials, recent research studies reveal that soluble mediators with proper redox potential could permit the charge storage within the electrolyte.<sup>20–22</sup> As a result, the introduction of suitable redox mediators at the cathode side of LICs could contribute to extra capacity through their redox reactions and the supererogatory loading mass of cathode materials could be essentially reduced.<sup>23–25</sup> Our latest work has constructed a LIC with equal mass loading of the two electrodes regulated by iodide species involved in the catholyte.<sup>26</sup>

Despite their great success in modulating the mass loading in LICs, redox mediators could easily lose the stored charges

State Key Laboratory of Heavy Oil Processing, Institute of New Energy, College of Chemistry and Chemical Engineering, China University of Petroleum (East China), Qingdao, 266580, China. E-mail: [hhu@upc.edu.cn](mailto:hhu@upc.edu.cn); [wumb@upc.edu.cn](mailto:wumb@upc.edu.cn)

† Electronic supplementary information (ESI) available. See <https://doi.org/10.1039/d2ta02256g>

due to their shuttle in the electrolyte, similar to the major obstacle observed in lithium-sulfur batteries.<sup>27–29</sup> Herein, we, for the first time, report the rational design of zeolitic imidazolate framework-7 (ZIF-7) particle-modified separators for LICs to resolve the concomitant shuttle effect of using redox mediators. The ZIF-7 modified separator was prepared by a blade-casting technique where ZIF-7 particles were firmly attached on one side of the traditional glass fiber (GF) separators. The permeation measurement shows that the iodide species could rapidly diffuse through the GF separator while their shuttle could be fundamentally terminated with the ZIF-7-modified separators employed. In contrast to the continuous fading of the extra capacity provided by the redox mediators in the system using the traditional separator, the employment of ZIF-7 modified separators could thus secure a stable output of the redox mediator-involved capacity. Based on the experimental and theoretical investigation, the restricted shuttle of the redox mediators is associated with physical obstruction and chemical interactions induced by the ZIF-7 particles. Then, the LICs were assembled using the nanostructured LTSO anode and AC cathode coupled with the LiI-involved catholyte separated by a ZIF-7 modified separator. The shuttle effect of soluble iodine species is then effectively alleviated, allowing a long cycling capability. Due to the regulated mass loading on both electrodes, the LICs constructed based on this idea afford a high energy density of 238.6 W h kg<sup>-1</sup> and power capability of 14 295.2 W kg<sup>-1</sup>.

## 2. Materials and methods

### 2.1 Materials and reagents

Commercial AC (C112241, CAS: 7440-44-0), titanium butoxide (purity ≥ 98%, CAS: 5593-70-4), tetraethyl orthosilicate (purity ≥ 99%, CAS: 78-10-4), lithium hydroxide monohydrate (purity ≥ 98%, CAS: 1310-66-3), dopamine hydrochloride (purity ≥ 98%, CAS: 62-31-7), multi-walled carbon nanotubes (MWCNTs) (purity ≥ 95%, CAS: 308 068-56-6), lithium iodide (purity ≥ 99%, L106780, CAS: 10377-51-2), and lithium nitrate (purity ≥ 99.9%, L100138, CAS: 7790-69-4) were purchased from Aladdin Industrial Corporation. Lithium bis-(trifluoromethanesulfonyl) imide (LiTFSI) (product number: 9100301) and diethylene glycol dimethyl ether (DEGDME) (product number: 9201801) were acquired from DoDoChem. All the chemicals were used as received without further purification. The deionized water (15 MΩ) was produced by using a Millipore system in our lab.

### 2.2 Preparation of the ZIF-7-modified separator

ZIF-7 particles were synthesized by a solvothermal method according to previous research.<sup>30</sup> In detail, 2.975 g of zinc nitrate hexahydrate (Zn(NO<sub>3</sub>)<sub>2</sub>·6H<sub>2</sub>O, Aladdin, 99%) and 9.451 g of benzimidazole (BIM, Aladdin, 98%) were dissolved in a mixed solvent containing 233.6 g of *N,N*-dimethylformamide (DMF) and 50.4 g of deionized water. After stirring for 2 hours, the solution was sealed in a Teflon-lined vessel and reacted at 130 °C for 72 h. The ZIF-7 particles were harvested *via* washing with DMF and ethanol several times, and then dried overnight

at 100 °C. ZIF-7 modified separators were prepared by a blade-casting technique. The obtained ZIF-7 particles and polyvinylidene fluoride (PVDF) were ground at a mass ratio of 3 : 1 with the aid of DMF. The well-ground slurry was then cast on the separator using an automatic coater. After drying at 80 °C for 12 h, the ZIF-7 modified separator was obtained.

### 2.3 Preparation of the kinetically favourable anode material

The anode material used in this work is a three-dimensional carbon encapsulated LTSO (3DC@LTSO), which was synthesized by a solid reaction method.<sup>31</sup> In detail, 6.8 g of titanium butoxide (C<sub>16</sub>H<sub>36</sub>O<sub>4</sub>Ti, Aladdin, 98%) and 4.2 g of tetraethyl orthosilicate (C<sub>8</sub>H<sub>20</sub>O<sub>4</sub>Si, Aladdin, 99%) were dissolved in 80 ml of ethanol to form solution A. Meanwhile, 1.7 g of lithium hydroxide monohydrate (LiOH·H<sub>2</sub>O, Aladdin, 98%) was dissolved in 80 ml of deionized water to generate solution B. Solution A was added into solution B dropwise under stirring along with introducing 7.6 g of dopamine hydrochloride (Aladdin, 98%) and 0.5 g of MWCNTs to generate a suspension. After drying, the obtained powder was annealed at 870 °C under a N<sub>2</sub>/Ar atmosphere for 8 hours to produce 3DC@LTSO.

### 2.4 Characterization

The morphology was observed using scanning electron microscopy (SEM, Hitachi S4800). The crystal structure was determined using X-ray diffraction (X' Pert PRO MPD). The nitrogen sorption isotherms were recorded on a physisorption analyzer (Micromeritics TriStar II 3020). The micropore size distribution was determined using the Horvath–Kawazoe method.

An H-type electrolytic cell was used for the penetration test. Different solutions were added to the two chambers of the electrolytic cell. Specifically, the left chamber contained an aqueous solution of 1 M LiI and 0.1 M I<sub>2</sub> to simulate polyiodide species, while the right chamber was filled with an aqueous solution of 0.5 M Li<sub>2</sub>SO<sub>4</sub> which is colorless. Separators including the ZIF-7 modified one and the traditional GF separator were used to separate the two chambers. The diffusion of polyiodide was recorded by observing the color change of the solution in the right chamber.

The density functional theory (DFT) calculations were performed using the VASP program to study the interaction of ZIF-7 with I<sub>2</sub>. The Perdew–Burke–Ernzerhof (PBE) functional under the generalized gradient approximation (GGA) was adopted. At the same time, the projector augmented wave (PAW) method was used to describe the electron–ion interaction, and the plane wave cut-off energy was set to 400 eV. Considering the periodic interactions, ZIF-7 and I<sub>2</sub> were placed in a cube of side length 25 Å for structural relaxation. The Monkhorst–Pack *k*-point is set as 2 × 2 × 2 and the convergence criteria for energy and force were set to 10<sup>-4</sup> eV and 0.02 eV Å, respectively. The adsorption energy (*E*<sub>ads</sub>) of iodine on the surface of the ZIF-7 material was calculated by using DFT:

$$E_{\text{ads}} = E_{\text{Total}} - E_{\text{ZIF-7}} - E_{\text{I}_2}$$

In this equation,  $E_{\text{Total}}$  is the total energy,  $E_{\text{I}_2}$  is the energy of  $\text{I}_2$ , and  $E_{\text{ZIF}}$  is the surface energy of ZIF-7.

### 2.5 Electrochemical measurements

The cells used in this work were assembled in a glove box filled with Ar. To fabricate the electrode, a slurry containing the electrode materials (80 wt%), carbon black (10 wt%), and PVDF (10 wt%) were prepared by grinding them with a few drops of NMP. The slurry was coated on the current collector by using an electric coater. The electrodes were obtained after vacuum drying at 80 °C for 12 h.

An asymmetric electrolyte design was employed in this work. The anolyte is composed of 1 M LITFSI in DEGDM. As for the catholyte, an extra of 50 mM LiI was introduced into the anolyte of 1 M LITFSI in DEGDM. To explore the electrochemical performance of the AC cathode, the half cells were fabricated using the lithium foil as the counter and reference electrodes and the ZIF-7 modified separator was used. The reference cells were also constructed using the GF separator.

To assemble the LICs, the cathode and anode were pre-treated *via* the following manner: the AC//Li and 3DC@LTSO//Li half cells were charged and discharged for 10 cycles at a current density of 0.1 A g<sup>-1</sup>, and then stabilized at 1.6 V *vs.* Li/Li<sup>+</sup> for 80 h. After that, the two half cells were disassembled. The pre-treated AC electrode was used as the cathode by adding 70 μl of catholyte and the 3DC@LTSO electrode served as the anode with 70 μl of anolyte. The ZIF-7 modified separator was inserted between the two electrodes. The mass ratio of the cathode and anode was set as 1 : 1.

The electrochemical performance of all cells was characterized using a Neware battery test system. Cyclic voltammetry (CV) and the galvanostatic charge and discharge (GCD) tests were conducted using an IVIUM multi-channel electrochemical workstation. All electrochemical measurements were conducted at 25 °C.

## 3. Results and discussion

Typically, the separator in electrochemical energy storage devices is to prohibit the direct contact of the two electrodes and secure the ion transfer.<sup>32,33</sup> As for the system with soluble redox mediators, the separator should further selectively prohibit the transfer of the soluble mediators since their transfer could result in serious self-discharge.<sup>34,35</sup> Recently, soluble redox mediators have been introduced into the LICs for capacity balancing. A typical example is the incorporation of LiI in the catholyte of LICs and the redox chemistry of LiI provides a viable means to regulate the mass loading at the cathode side.<sup>26</sup> Nevertheless, soluble LiI and their intermediate species including  $\text{I}_3^-$ , could directly transfer through the pores of the typical separator, resulting in the loss of capacity. The recent booming interest in lithium–sulfur batteries suggests that the incorporation of an interlayer in the separator with suitable porosity could essentially address this issue.<sup>36,37</sup> Among all the potential candidates, metal–organic frameworks (MOFs) represent a promising choice of materials due to their adjustable

porous structures.<sup>38–40</sup> The key reason is that these unique frameworks can provide nanoporous and crystalline structures that facilitate charge-involved reactions.<sup>41,42</sup> Theoretically, the homogeneous pores of these frameworks can be precisely controlled, thereby exhibiting enhanced molecular and ionic sieving capabilities. These features render MOF-based nanomaterials great potential in electrochemical systems.<sup>43–45</sup>

Based on this inspiration, the separator was modified with a ZIF-7 interlayer (Fig. 1) *via* a simple blade-casting process. The as-prepared ZIF-7 particles (Fig. S1†) and PVDF were mixed with the aid of DMF to produce a slurry. Then, the slurry was cast on the separator with an electronic-controlled blade as illustrated in Fig. 2a. After removing the residual solvent, the ZIF-7 modified separator was obtained. The ZIF-7 particles (Fig. 2b and S2a†) with a plate-like morphology of several tens of micrometers are uniformly and firmly loaded on the surface of the GF separator and the thickness of the ZIF-7 interlayer is around 300 μm (Fig. 2c and S2b†). The reason for selecting ZIF-7 is mainly based on its suitable pore size.<sup>46,47</sup> The pore size of ZIF-7 is mainly located at 0.9 nm, as reflected in Fig. 2d. Although the size of the iodine/iodide ions (Fig. S3†) is smaller than the pore size of ZIF-7, the iodide species are usually aggregated with a size of more than 1 nm.<sup>48,49</sup> Compared to the several tens of micrometer-sized particles, the direct diffusion of the iodine species through the micro-porous structure could be largely prohibited without affecting the transfer of other species.<sup>48,49</sup> In addition, ZIF-7 could exert mild chemical adsorption towards the iodine species as reflected from the DFT calculations (Fig. 2e,f). According to the difference charge density (Fig. 2f), the electron depletion region was distributed on the surface of ZIF-7 in contact with iodine species, indicating the occurrence of electron transfer, and that electrons were transferred from ZIF-7 to iodine species. Meanwhile, the electron loss region within the iodine species proved that the bonding state was reduced, promoting the dissociation of iodine species for facilitated electrochemical processes.<sup>50</sup> Such a chemical interaction could mildly draw the active species while prohibiting the strong anchoring of them. As a result, the possible intergranular migration could be alleviated.

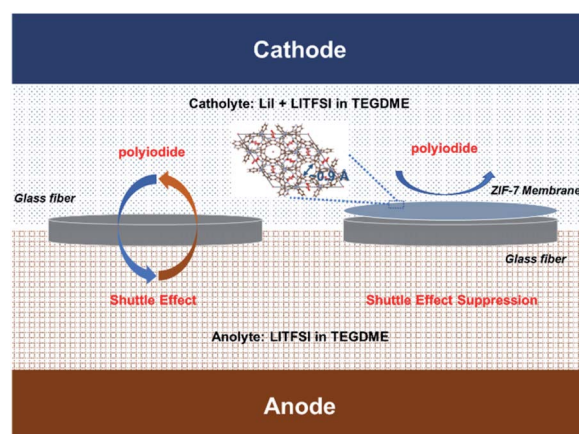


Fig. 1 Schematic illustrations of ZIF-7 modified separators for prohibiting the shuttling of redox mediators.

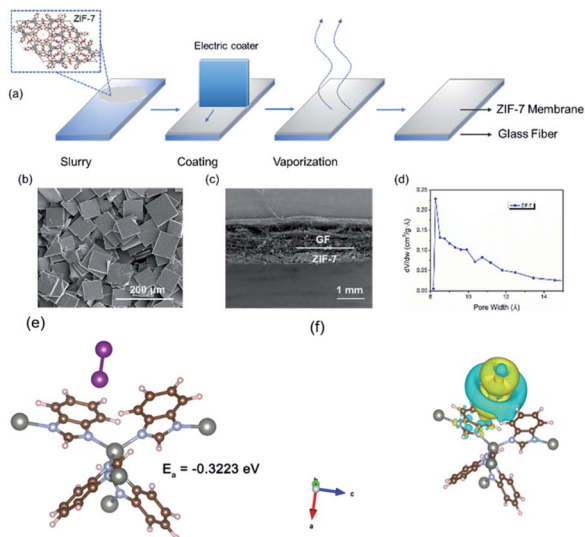


Fig. 2 (a) The fabrication process of ZIF-7 modified separators. (b) SEM image of ZIF-7 loaded on the separator. (c) SEM image of the cross-section of a modified separator. (d) Pore-size distribution curve of ZIF-7. (e) The adsorption energy of  $I_2$  on ZIF-7. (f) Difference charge density of  $I_2$  adsorption on ZIF-7.

To visually detect the suppression of iodine-involved shuttling, an H-type electrolytic cell containing different solutions in the two chambers was designed.<sup>49</sup> As shown in Fig. 3a, the left chamber containing polyiodide species (an aqueous solution of 1 M LiI and 0.1 M  $I_2$ ) is brown while the right chamber is colorless with a 0.5 M aqueous solution of  $Li_2SO_4$ . By separating the two chambers with the traditional separator, the gradual diffusion of polyiodide was observed as the color is changed in the right chamber. In contrast, when the ZIF-7 modified separator was used, the right chamber remained colorless even after standing for 1 day (Fig. 3b). To evaluate the effect of the ZIF-7 modified separator in electrochemical processes, the half-cells with AC as the working electrode, lithium foil as the reference and counter electrodes, and LiI as the additive in the catholyte were fabricated. As shown in Fig. 3c, the cell was charged with a constant current to 4.2 V vs.  $Li/Li^+$  to completely convert iodide into polyiodide. Different aging duration gradients of 0.5, 1, 2, and 3 h were set to analyze the capacity loss.<sup>49</sup> As the duration increases, the irreversible capacity of the cell with the traditional separator in the discharge process increases accordingly, confirming that the shuttle of redox mediators has caused serious self-discharge. On the other hand, the capacity loss of the cell using the ZIF-7 modified separator remains at an acceptable level of less than 5%. The almost overlapped discharge curves at different durations indicate that the ZIF-7 modified separator could effectively block the shuttle of the iodine species, giving rise to improved stability. The effect of the ZIF-7 modified separator could be further confirmed by the coulombic efficiency (CE). As shown in Fig. 3d, the CE of the cell with the traditional separator decreases as the aging time increases. When the aging time reaches 5 h, the CE decreases to 75%. In contrast, the CE of the cell using the ZIF-7 modified separator remains almost unchanged with a short duration.

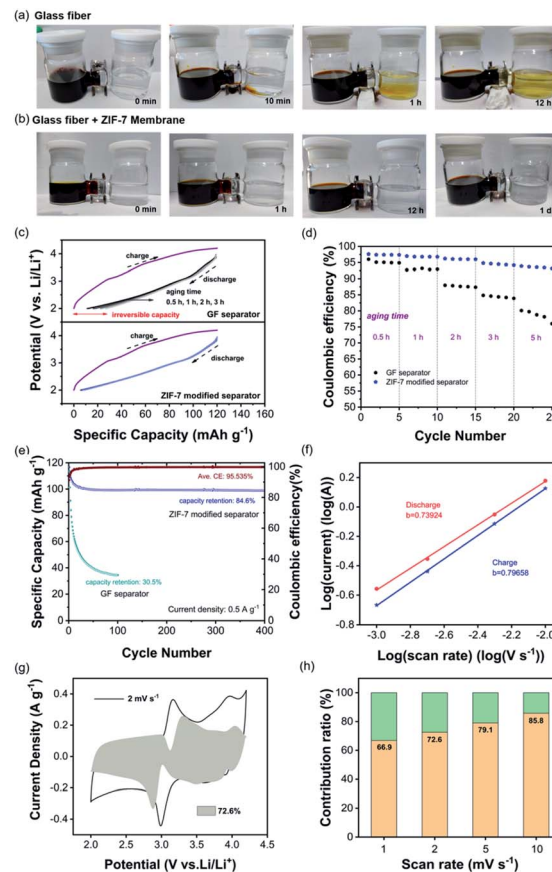


Fig. 3 Optical images of an H-type electrolytic cell with an aqueous solution of 1 M LiI and 0.1 M  $I_2$  in the left chamber and a 0.5 M  $Li_2SO_4$  aqueous solution using a GF separator (a) and a ZIF-7 modified separator (b). (c) Electrochemical aging test (from 0.5 to 3 hours resting after fully charging) for half cells with the AC working electrodes using a GF separator (upper) and a ZIF-7 modified separator (lower) at  $0.5 \text{ A g}^{-1}$ . (d) CE of the cells with a GF separator and a ZIF-7 modified separator at different aging durations. (e) Long-term cycling stability of the cells with a GF separator and a ZIF-7 modified separator. (f)  $\log(i)$  versus  $\log(\nu)$  plots at specific peak currents. (g) CV curve with the calculated pseudocapacitive fraction shown by the shaded area at  $2 \text{ mV s}^{-1}$ . (h) Bar chart showing the percentage of the calculated pseudocapacitive contribution at  $1.0$ – $10.0 \text{ mV s}^{-1}$ .

Even after aging for 5 h, the CE is still larger than 90%. Because of the efficiently suppressed shuttling of iodine species, the cell with a ZIF-7 modified separator can achieve excellent capacity retention after 400 cycles at a relatively low current density ( $0.5 \text{ A g}^{-1}$ ), as shown in Fig. 3e. The CV profiles in Fig. S4† exhibit two pairs of reversible redox peaks associated with the iodide-involved conversion. To evaluate the stability of the ZIF-7 particles, the cells were disassembled after long-term cycling and particles were scraped off from the modified separators. The ZIF-7 particles still maintained the original morphology after long-term cycling (Fig. S5†). Furthermore, as shown in Fig. S6,† the surface of the lithium foil in the cell without a ZIF-7 interlayer has largely deteriorated while the one with a modified separator shows a smooth surface.

Then, the kinetic performance of the iodine-involved redox chemistry was analyzed using the power law. The cell employing

the ZIF-7-modified separator was evaluated at scan rates ranging from 1.0 to 10.0 mV s<sup>-1</sup> and the CV curves are shown in Fig. S7.† The area of the CV curve increases with the scan rate, and the reduction and oxidation peaks shift to lower and higher potentials, respectively owing to the polarization effect.<sup>51</sup> The iodine-involved reactions are generally slow in kinetics.<sup>52</sup> To explore their effect on the rate capability of the cathode, the kinetic capability of the cell with the LiI-involved catholyte was evaluated by using eqn (1) and (2)<sup>53</sup>:

$$i = av^b \quad (1)$$

$$\log(i) = b \log(v) + \log(a) \quad (2)$$

where  $i$  is the current at a scan rate of  $v$  while  $a$  and  $b$  are tunable parameters. The  $b$  value is generally fitted between 0.5 and 1, and a  $b$  value of 1 indicates the full capacitive contribution and  $b = 0.5$  corresponds to the totally diffusion-controlled process. The  $b$  value is obtained by calculating the slope of the  $\log(i)$  versus  $\log(v)$  plot, as shown in Fig. 3f. The  $b$ -values during charge and discharge are 0.797 and 0.739, respectively, indicating that the capacity is a combination of pseudocapacitive contribution and ion diffusion. Then, the reversible capacity is divided into pseudocapacitive contribution and diffusion contribution according to eqn (3) and (4)<sup>54</sup>:

$$i = k_1v + k_2v^{1/2} \quad (3)$$

$$i/v^{1/2} = k_1v^{1/2} + k_2 \quad (4)$$

The pseudocapacitive and diffusion contributions are measured with  $k_1$  and  $k_2$ , respectively. As shown in Fig. 3g, the shadow area represents the contribution of pseudocapacitance, accounting for 72.4%. Overall, the histogram shows that the pseudocapacitive contribution increases from 66.9% to 85.8% at current density gradients of 1.0–10.0 mV s<sup>-1</sup> (Fig. 3h), indicating fast reaction kinetics during redox processes.<sup>55</sup>

To assess the practical performance of the ZIF-7 modified separator, the LICs were assembled using 3DC@LTSO as the anode and AC as the cathode, which was separated by a ZIF-7 modified separator. Of particular note is that the loading mass of the cathode and anode is equal as the capacity gap is balanced by the introduction of LiI in the catholyte. Meanwhile, the kinetics imbalance is largely reduced through constructing highly conductive electrode materials. The nanostructured LTSO was *in situ* mixed with MWCNTs, as illustrated in Fig. S8.† The electrochemical performance of the 3DC@LTSO electrode is shown in Fig. S9.† The specific capacity of 3DC@LTSO has approached more than 300 mA h g<sup>-1</sup> with a slope-like GCD curve, indicating the excellent rate capability. In addition, the nanostructured LTSO electrodes also exhibit excellent cycle performance, with a capacity retention rate of 84.0% after 1500 cycles, ensuring the long cycle life of the capacitor. To effectively utilize the working voltage window of the electrolyte, the initial working potential ( $E_{OV}$ ) of the cathode and anode was regulated to 1.6 V vs. Li/Li<sup>+</sup>.<sup>56</sup> Based on the optimal working potential window, the cathode could operate using the dual ion adsorption mechanism along with the redox chemistry of iodine

species, as reflected in Fig. S10.† In this case, the capacity of the cathode is similar to that of the anode, thus permitting equal mass loading on both electrodes. The CV curve of the LIC with the ZIF-7 modified separator after 100 cycles is shown in Fig. 4a. When compared, the one with the GF separator exhibits a decreased area indicating the loss of the iodine species. Moreover, the CV curves of the two LICs over cycles were compared and are shown in Fig. S11.† An obvious area shrinkage in the CV curves is observed for the one using the GF separator while its counterpart with the ZIF-7 modified separator offers almost overlapped curves during the same CV measurements. In addition, the three-electrode split cell was also assembled where the GCD curves and the potential variation of both electrodes could be simultaneously recorded. As shown in Fig. 4b, all three curves exhibit a triangular shape, indicating good reversibility and the well-match electrodes. The LIC was tested at different current densities from 0.1 to 5.0 A g<sup>-1</sup> and all the GCD curves give a triangular shape (Fig. 4c). Then, the specific capacitance of the electrodes was calculated at different current densities and is illustrated in Fig. 4d. The LIC employing the ZIF-7-modified separator offers larger specific capacitances and higher CE at all the tested current densities compared to the LIC with the GF separator. Moreover, the modified separator could largely extend the cycling life of LICs where a high capacity retention of 85% could be secured even after 4000 cycles. At the same time, the capacity decreases to 30% for the traditional one only after 150 cycles. The Ragone plot is shown in Fig. 4f and was compared with the previous

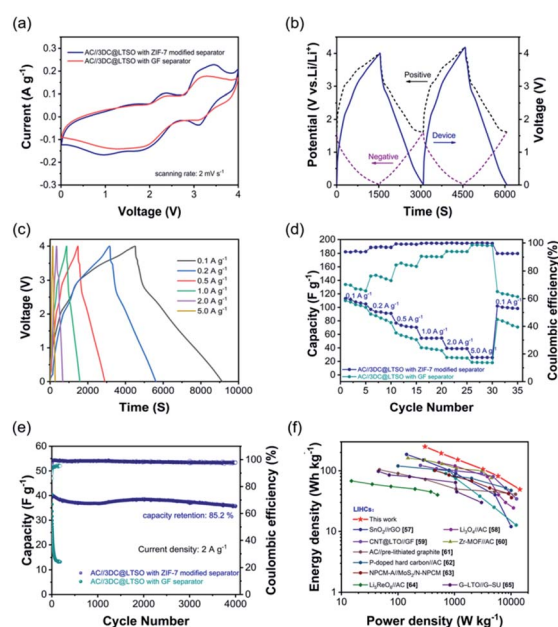


Fig. 4 Electrochemical performance of AC//3DC@LTSO LICs. (a) CV curves of AC//3DC@LTSO LICs with traditional and ZIF-7 modified separators. (b) The GCD curves of the AC//3DC@LTSO LIC with a ZIF-7 modified separator recorded using a three-electrode split cell. (c) GCD curves at different current densities. (d) Rate performance and (e) long-term cycling stability comparison of the two types of LICs. (f) Ragone plots of the AC//3DC@LTSO LIC using a ZIF-7 modified separator and other related publications.<sup>57–65</sup>

results. The LICs could achieve an energy density of 238.56 W h kg<sup>-1</sup> and a large power density of 14 295.2 W kg<sup>-1</sup> by virtue of the reversible and stable additional pseudo-capacity provided by redox mediators, far superior to many of the previous reports.

## 4. Conclusion

A MOF-modified separator has been introduced into LICs, facilitating the use of redox mediators. Specifically, the redox mediators provide extra capacity, allowing equal mass loading, a highly desired electrode configuration, and prohibit the typical shuttle effect in this design. By rationally constructing an interlayer on the separator using MOFs with a suitable pore size and surface chemistry, the shuttle of LiI could be simultaneously resolved through physical obstruction and mild chemical attraction. Because of these effects, the LiI-involved extra capacity offers high reversibility, thus a long-term cycling performance. Then, the as-fabricated LICs with the modified separator offer a high CE, high energy density, and long-term cycling performance. The strategy proposed here may inspire new design rationales for high-performance LICs.

## Author contributions

The manuscript was written through contributions of all authors. All authors have given approval to the final version of the manuscript.

## Conflicts of interest

There are no conflicts to declare.

## Acknowledgements

Financial support from the National Natural Science Foundation of China (22179145, 21975287, and 22138013), Shandong Provincial Natural Science Foundation (ZR2020ZD08), the startup support grant from China University of Petroleum (East China), and Taishan Scholar Project (No. ts201712020) is appreciated.

## Notes and references

- J. M. Dieterich and E. A. Carter, *Nat. Rev. Chem.*, 2017, **1**, 0032.
- I. Gunnarsdottir, B. Davidsdottir, E. Worrell and S. Sigurgeirsdottir, *Renewable Sustainable Energy Rev.*, 2021, **141**, 110770.
- J. Wang, H. Kong, J. Zhang, Y. Hao, Z. Shao and F. Ciucci, *Prog. Mater. Sci.*, 2021, **116**, 100717.
- J. Lu, T. Wu and K. Amine, *Nat. Energy*, 2017, **2**, 17011.
- M. Waqas, S. Ali, C. Feng, D. Chen, J. Han and W. He, *Small*, 2019, **15**, e1901689.
- N. Choudhary, C. Li, J. Moore, N. Nagaiah, L. Zhai, Y. Jung and J. Thomas, *Adv. Mater.*, 2017, **29**, 1605336.
- W. Raza, F. Ali, N. Raza, Y. Luo, K.-H. Kim, J. Yang, S. Kumar, A. Mehmood and E. E. Kwon, *Nano Energy*, 2018, **52**, 441–473.
- G. G. Amatucci, F. Badway, A. Du Pasquier and T. Zheng, *J. Electrochem. Soc.*, 2001, **148**, A930.
- Z. Weng, F. Li, D. W. Wang, L. Wen and H. M. Cheng, *Angew. Chem., Int. Ed.*, 2013, **52**, 3722–3725.
- M. Yu, D. Lin, H. Feng, Y. Zeng, Y. Tong and X. Lu, *Angew. Chem., Int. Ed.*, 2017, **56**, 5454–5459.
- R. Wang, P. Liu, J. Lang, L. Zhang and X. Yan, *Energy Storage Mater.*, 2017, **6**, 53–60.
- S. Zheng, Z. Wu, S. Wang, H. Xiao, F. Zhou, C. Sun, X. Bao and H. Cheng, *Energy Storage Mater.*, 2017, **6**, 70–97.
- A. M. Glushenkov and A. V. Ellis, *Adv. Sustainable Syst.*, 2018, **2**, 1800006.
- Y. Han, Y. Lu, S. Shen, Y. Zhong, S. Liu, X. Xia, Y. Tong and X. Lu, *Adv. Funct. Mater.*, 2019, **29**, 1806329.
- Y. Mei, Y. Li, F. Li, Y. Li, Y. Jiang, X. Lan, S. Guo and X. Hu, *J. Mater. Sci. Technol.*, 2020, **57**, 18–25.
- K. Jayaramulu, D. P. Dubal, B. Nagar, V. Ranc, O. Tomanec, M. Petr, K. K. R. Datta, R. Zboril, P. Gomez-Romero and R. A. Fischer, *Adv. Mater.*, 2018, **30**, e1705789.
- B. Yang, J. Chen, L. Liu, P. Ma, B. Liu, J. Lang, Y. Tang and X. Yan, *Energy Storage Mater.*, 2019, **23**, 522–529.
- K. L. Van Aken, M. Beidaghi and Y. Gogotsi, *Angew. Chem., Int. Ed.*, 2015, **54**, 4806–4809.
- B. Akinwolemiwa, C. Wei, Q. Yang, L. Yu, L. Xia, D. Hu, C. Peng and G. Z. Chen, *J. Electrochem. Soc.*, 2018, **165**, A4067–A4076.
- Q. Wang, Y. Nie, X. Chen, Z. Xiao and Z. Zhang, *J. Power Sources*, 2016, **323**, 8–16.
- L. Hu, C. Shi, K. Guo, T. Zhai, H. Li and Y. Wang, *Angew. Chem., Int. Ed.*, 2018, **57**, 8214–8218.
- J. Lee, S. Choudhury, D. Weingarh, D. Kim and V. Presser, *ACS Appl. Mater. Interfaces*, 2016, **8**, 23676–23687.
- D. Xu, W. Hu, X. N. Sun, P. Cui and X. Y. Chen, *J. Power Sources*, 2017, **341**, 448–456.
- H. Yu, J. Wu, L. Fan, S. Hao, J. Lin and M. Huang, *J. Power Sources*, 2014, **248**, 1123–1126.
- L. Chen, H. Bai, Z. Huang and L. Li, *Energy Environ. Sci.*, 2014, **7**, 1750–1759.
- Y. Zhang, H. Chao, H. Liu, X. Wang, W. Xing, H. Hu and M. Wu, *Chem. Commun.*, 2020, **56**, 12777–12780.
- Z. Li, H. B. Wu and X. W. Lou, *Energy Environ. Sci.*, 2016, **9**, 3061–3070.
- J. Zhang, H. Hu, Z. Li and X. W. Lou, *Angew. Chem., Int. Ed.*, 2016, **55**, 3982–3986.
- W. Jing, J. Zu, K. Zou, X. Dai, Y. Song, J. Han, J. Sun, Q. Tan, Y. Chen and Y. Liu, *J. Mater. Chem. A*, 2022, **10**, 4833–4844.
- X. Ma, X. Wu, J. Caro and A. Huang, *Angew. Chem., Int. Ed.*, 2019, **58**, 16156–16160.
- J. Liu, W. K. Pang, T. Zhou, L. Chen, Y. Wang, V. K. Peterson, Z. Yang, Z. Guo and Y. Xia, *Energy Environ. Sci.*, 2017, **10**, 1456–1464.
- M. Rana, M. Li, X. Huang, B. Luo, I. Gentle and R. Knibbe, *J. Mater. Chem. A*, 2019, **7**, 6596–6615.
- M. Zou, Y. Luo, X. Ma, J. Fan, Y. Niu, J. Liang and G. Gong, *J. Membr. Sci.*, 2021, **637**, 119597.

- 34 B. Evanko, S. W. Boettcher, S. J. Yoo and G. D. Stucky, *ACS Energy Lett.*, 2017, **2**, 5281–5290.
- 35 M. Z. Yang Huang, Z. Lin, B. Zhao, S. Zhang, J. Yang, C. Zhu, D. S. Heng Zhang and Y. Shib, *J. Mater. Chem. A*, 2015, **3**, 10910–10918.
- 36 X. Li, Y. Zhang, S. Wang, Y. Liu, Y. Ding, G. He, N. Zhang and G. Yu, *Nano Lett.*, 2020, **20**, 701–708.
- 37 H. Li, Y. Zhou, M. Zhao, B. Jin, Z. Wen, H. Xie, S. Dou and Q. Jiang, *Adv. Energy Mater.*, 2020, **10**, 1902695.
- 38 B. Y. Guan, L. Yu and X. W. Lou, *Energy Environ. Sci.*, 2016, **9**, 3092–3096.
- 39 J. E. Bachman, Z. P. Smith, T. Li, T. Xu and J. R. Long, *Nat. Mater.*, 2016, **15**, 845–849.
- 40 H. Song, L. Shen, J. Wang and C. Wang, *J. Mater. Chem. A*, 2016, **4**, 15411–15419.
- 41 X. Yang, C. Lin, D. Han, G. Li, C. Huang, J. Liu, X. Wu, L. Zhai and L. Mi, *J. Mater. Chem. A*, 2022, **10**, 3989–3995.
- 42 K. Zhang, K. O. Kirlikovali, R. S. Varma, Z. Jin, H. W. Jang, O. K. Farha and M. Shokouhimehr, *ACS Appl. Mater. Interfaces*, 2020, **12**, 27821–27852.
- 43 K. Zhang, K. O. Kirlikovali, Q. V. Le, Z. Jin, R. S. Varma, H. W. Jang, O. K. Farha and M. Shokouhimehr, *ACS Appl. Nano Mater.*, 2020, **3**, 3964–3990.
- 44 W. Yan, K. Fan, L. Zheng and Z. Jin, *Small Struct.*, 2021, **2**, 2100122.
- 45 W. Yan, J. Su, Z. Yang, S. Lv, Z. Jin and J. Zuo, *Small*, 2021, **17**, e2005209.
- 46 X. Wang, Y. Zhao, F. Wu, S. Liu, Z. Zhang, Z. Tan, X. Du and J. Li, *J. Energy Chem.*, 2021, **57**, 19–27.
- 47 W. Cai, T. Lee, W. Cho, D. Han, N. Choi, A. Yip and J. Choi, *J. Am. Chem. Soc.*, 2014, **136**, 7961–7971.
- 48 Y. Wang, L. Song, F. Li, Y. Wang, X. Wang, M. Li, L. Zou and J. Xu, *J. Power Sources*, 2021, **492**, 229575.
- 49 H. Yang, Y. Qiao, Z. Chang, H. Deng, P. He and H. Zhou, *Adv. Mater.*, 2020, **32**, e2004240.
- 50 Z. Su, Z. Wei, C. Lai, H. Deng, Z. Liu and J. Ma, *Energy Storage Mater.*, 2018, **140**, 129–135.
- 51 P. He, M. Yan, G. Zhang, R. Sun, L. Chen, Q. An and L. Mai, *Adv. Energy Mater.*, 2017, **7**, 1601920.
- 52 Li, B. Lin, Q. Li, H. Wang, S. Zhang and C. Deng, *ACS Appl. Mater. Interfaces*, 2017, **9**, 20508–20518.
- 53 D. Chao, C. Zhu, P. Yang, X. Xia, J. Liu, J. Wang, X. Fan, S. V. Savilov, J. Lin, H. J. Fan and Z. X. Shen, *Nat. Commun.*, 2016, **7**, 12122.
- 54 V. Augustyn, J. Come, M. A. Lowe, J. W. Kim, P. L. Taberna, S. H. Tolbert, H. D. Abruna, P. Simon and B. Dunn, *Nat. Mater.*, 2013, **12**, 518–522.
- 55 P. He, Y. Quan, X. Xu, M. Yan, W. Yang, Q. An, L. He and L. Mai, *Small*, 2017, **13**, 1702551.
- 56 H. Qin, H. Chao, M. Zhang, Y. Huang, H. Liu, J. Cheng, L. Cao, Q. Xu, L. Guan, X. Teng, Y. Li, K. Wang, H. Guo, H. Hu and M. Wu, *Carbon*, 2021, **180**, 110–117.
- 57 J. Ajuria, M. Arnaiz, C. Botas, D. Carriazo, R. Mysyk, T. Rojo, A. V. Talyzin and E. Goikolea, *J. Power Sources*, 2017, **363**, 422–427.
- 58 L. Shen, H. Lv, S. Chen, P. Kopold, P. A. Aken, X. Wu, J. Maier and Y. Yu, *Adv. Mater.*, 2017, **29**, 1700142.
- 59 Y. Liu, W. Wang, J. Chen, X. Li, Q. Cheng and G. Wang, *J. Energy Chem.*, 2020, **50**, 344–350.
- 60 W. Yan, J. Su, Z. Yang, S. Lv, Z. Jin and J. Zuo, *Small*, 2021, **17**, 2005209.
- 61 P. Sennu, V. Aravindan, M. Ganesan, Y. Lee and Y. Lee, *ChemSusChem*, 2016, **9**, 849–854.
- 62 Z. Yang, Y. Gao, Z. Zhao, Y. Wang, Y. Wu and X. Wang, *J. Power Sources*, 2020, **474**, 228500.
- 63 J. Jiang, Y. Zhang, Y. An, L. Wu, Q. Zhu, H. Dou and X. Zhang, *Small Struct.*, 2019, **3**, 1900081.
- 64 P. Jeżowska, K. Fic, O. Crosnier, T. Brousse and F. Béguina, *J. Mater. Chem. A*, 2016, **4**, 12609–12615.
- 65 K. Leng, F. Zhang, L. Zhang, T. Zhang, Y. Wu, Y. Lu, Y. Huang and Y. Chen, *Nano Res.*, 2013, **6**, 581–592.